Article

pubs.acs.org/JPCB

1 Topological Origins of the Mixed Alkali Effect in Glass

- ² Collin J. Wilkinson,[†] Arron R. Potter,[‡] Rebecca S. Welch,[¶] Caio Bragatto,[¶] Qiuju Zheng,[§]
 ³ Mathieu Bauchy,[∥]
 ⁶ Mario Affatigato,[¶] Steven A. Feller,[¶] and John C. Mauro*,[†]
 ⁶
- ⁴ Department of Materials Science and Engineering, The Pennsylvania State University, University Park, Pennsylvania 16802, United
- 5 States

10

11

12

13

14

15

16

17

18

19

20

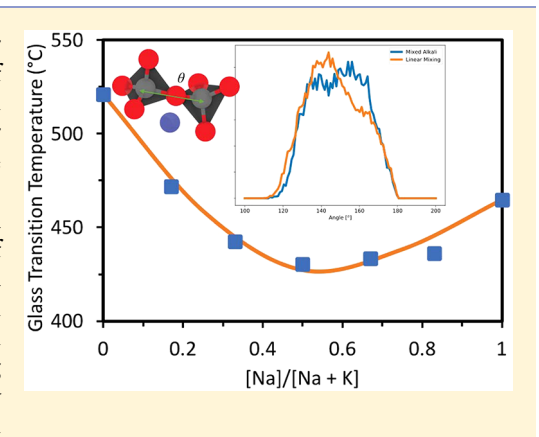
21

22

23

- 6 [‡]Department of Materials Science and Engineering, Rensselaer Polytechnic Institute, Troy, New York 12180, United States
- ⁷ Department of Physics, Coe College, Cedar Rapids, Iowa 52402, United States
- 8 School of Materials Science and Engineering, Qilu University of Technology, Jinan, 250353, China
- ⁹ Department of Civil and Environmental Engineering, University of California, Los Angeles, California 90095, United States

ABSTRACT: The mixed alkali effect, the deviation from expected linear property changes when alkalies are mixed in a glass, remains a point of contention in the glass community. While several earlier models have been proposed to explain mixed alkali effects on ionic motion, models based on or containing discussion of structural aspects of mixed-alkali glasses remain rare by comparison. However, the transition-range viscosity depression effect is many orders in magnitude for mixed-alkali glasses, and the original observation of the effect (then known as the Thermometer Effect) was of the highly anomalous temperature dependence of stress and structural relaxation time constants. With this in mind, a new structural model based on topological constraint theory is proposed herein which elucidates the origin of the mixed alkali effect as a consequence of network strain due to differing cation radii. Discussion of literature models and data alongside new molecular dynamics simulations and experimental data are presented in support of the model, with good agreement.



INTRODUCTION

26 The mixed alkali effect (MAE) was originally discovered in 1883 by Weber as part of his investigation of the 28 Thermometer Effect, wherein a glass containing significant 29 content of more than one alkali modifier undergoes unusually 30 fast low-temperature relaxation, altering the calibration of a 31 thermometer composed of such glass. The MAE manifests 32 as a nonadditivity of many glass properties as the ratio of one 33 alkali to the other changes and appears in a wide variety of 34 properties. Furthermore, one glass system may exhibit the 35 MAE for some property but another system may not, e.g., glass 36 transition temperature $(T_{\rm g})$ in silicates (significant effects) $^{4-8}$ 37 and borates (lesser effects). $^{9-11}$

Since its discovery, several models have been proposed to describe the MAE, to varying degrees of success. In many cases, models predicated purely on electrical properties fail to accurately predict changes in mechanical or thermal properties. 11

Major MAE Phenomena. As noted above, the mixed alkali effect was first observed experimentally in the unusually fast relaxation of thermometer glass. Since then, other mechanical and thermomechanical glass properties have also been found to exhibit a mixed alkali effect. One of the largest of these is found in the transformation-range viscosities of silicate glasses, which can be represented by their accordingly depressed glass transition temperatures $(T_{\rm g})$.

friction also shows a significant mixed-alkali effect, exhibiting 51 large peaks associated with coordinated rearrangement of alkali 52 ions in mixed-alkali glasses, which correlates in magnitude with 53 the slower ion diffusivity and maximizes where diffusivities are 54 equal. 10,11,17,18

Mixed-alkali glasses also show some deviations in other 56 mechanical properties. ^{10,11} Of particular modern importance 57 due to the recent popularity of ion-exchanged glass products 58 (some, e.g., ^{19,20} even utilizing ion exchange to examine the 59 MAE itself), the hardness of mixed-alkali glasses has been 60 shown to exhibit a moderate positive MAE. ^{11,21,22}

Although the original observation of the MAE was 62 thermomechanical, the effect is now perhaps best known for 63 its orders-of-magnitude changes in DC electrical conductivity 64 and ionic diffusivity. ^{10,11} Jain et al. ^{23,24} found that the 65 activation energy for DC electrical conduction increases in 66 mixed-alkali silicate glasses by almost a factor of 2; this leads to 67 correspondingly large effects in the conductivities themselves, 68 an effect noted across multiple glass systems. ^{10,11,23–25} The 69 MAE in conductivity diminishes with temperature and 70 frequency of the applied field, however, suggesting that local 71

Received: July 9, 2019 Revised: August 1, 2019 Published: August 1, 2019



72 motion is uninhibited but long-range motion is more difficult 73 in these systems. 9-11,26

The diffusivities of alkali ions exhibit a "crossover", a 75 common occurrence in mixed-alkali glasses where the majority 76 ion may limit the diffusivity of the minority ion, drastically 77 reducing its mobility. 10,11,23–25,27–29 Notably, cesium is a large 78 ion for which diffusion is rather difficult, yet there exists a 79 composition range in which the minority sodium ions are the 80 slower-diffusing cation species. 23 Day and Isard both also note 81 that the dielectric constant and loss are both significantly 82 diminished, in accordance with diminishing alkali mobilis 83 ties. 10,11

Recent Experimental Results. Greaves and Ngai³⁰ found via 85 X-ray absorption fine structure (XAFS) experiments that 86 alkalies in mixed-alkali silicate glasses do exhibit a tendency 87 toward local clustering, but those clusters generally appear to 88 be well-mixed in composition. They also suggest that alkali— 89 alkali interactions likely occur indirectly through differing 90 structural effects of each alkali.³⁰

Swenson et al.³¹ and Swenson and Adams³² conducted neutron and X-ray diffraction experiments on mixed-alkali phosphate glasses and used reverse Monte Carlo analysis to determine the structure of those glasses. Glass structure *local* to the alkali ions was largely unchanged between mixed- and single-alkali glasses and alkalies were found to have mixed randomly, supporting the conclusions of Greaves and Ngai.^{30–32}

The far-infrared (FIR) spectroscopy of Kamitsos et al.³³ 100 revealed that structural peaks associated with alkali-oxygen 101 bonds are shifted in mixed-alkali borate glasses relative to those 102 in single-alkali borate glasses. Large ion peaks decreased in 103 wavenumber and small ion peaks increased, suggesting that 104 small ion bonding is strengthened in mixed-alkali glasses. Large 105 ion bonding, by contrast, is weakened. Importantly, this study 106 found that the FIR spectra for mixed-alkali borate could not be 107 reproduced by any linear combination of single-alkali spectra.³ Sen et al.³⁴ noted that ⁷Li and ²³Na spin-lattice relaxation 109 times (T_1) reach their minimum value at much higher 110 temperatures for mixed-alkali silicate glasses than for single-111 alkali silicate glasses. They suggest that this is due to a smaller 112 effective number of hopping sites through which to diffuse. 113 This also increases the high-energy cutoff for the percolation 114 process responsible for DC conductivity.³⁴

Tomozawa and co-workers^{19,20,35} found that mixed alkali glasses have large, negative enthalpies of mixing, which may be replained by strong alkali—alkali interactions and local replained by strong alkali—alkali interactions and local Stress formed in ion-exchanged glass alters this enthalpy of mixing, and may induce ordering in the glass. The replaced the prevalence of alkali—alkali glasses effectively reduces the prevalence of alkali—alkali interactions since alkalies are consumed by charge compensating aluminum ions.

Recent Computational Results. Habasaki and Ngai³⁶ performed molecular dynamics simulations of mixed-alkali performed molecular dynamics simulations of mixed-alkali silicates. It was shown that for a short time after a site is the transportation of one type do not enter the sites of the other until sufficient relaxation has taken place. This work found that stress from mismatched sites causes depressed ionic conductivity in mixed-alkali glasses and results in greater coupling of ionic motion behavior to the network for mixed-transportation of more than one alkali ion were made more difficult in mixed-alkali glasses. The study also noted that more difficult in mixed-alkali glasses.

Huang and Cormack^{37–39} performed molecular dynamics 135 on sodium, potassium, and sodium-potassium silicate glasses. 136 Their radial distribution functions show good agreement with 137 literature values and note alkali clustering with random mixing 138 of alkalies in accordance with the later experiments of Greaves 139 and Ngai.30 They found that small ions bind more tightly, 140 though the majority ions exert some degree of control over the 141 glass structure. However, the overall site distributions for each 142 alkali in mixed-alkali glasses are narrower than in single-alkali 143 glasses, and their reported Si-O-Si bond angle distributions 144 exhibit significant bimodality compared to an expected additive 145 relation in mixed-alkali glasses. They argue that these results 146 support a conclusion later backed experimentally by Greaves 147 and Ngai; namely, that the MAE is largely structural in 148 origin. ^{30,37–39} Yu et al. further confirmed the structural origins 149 of the MAE by performing molecular dynamics simulations of 150 mixed-alkali silicates as well, showing significant stress on the 151 constituent alkali ions (see the following section).40

Theoretical Models. Yu et al.⁴⁰ proposed local instabilities 153 as a possible origin of the MAE vis-â-vis the thermometer effect 154 and showed via molecular dynamics simulations a compressive 155 stress exerted by the glass network on the alkali contained 156 within.⁴¹ Taking into account the relatively high deformability 157 of the oxygen ion electron cloud discussed by Anderson and 158 Stuart,⁴² the presence of nontrivial structural deformation as a 159 result seems quite plausible.

This is supported by LaCourse, ⁴³ who suggested that mixed- ¹⁶¹ alkali Si–O–Si bonds would be under strain, and again ¹⁶² considering the deformability of the oxygen electron cloud, this ¹⁶³ deformation would increase in mixed-alkali glasses. ^{29,42,43} ¹⁶⁴ LaCourse also argued that ionic conductivity is well-modeled ¹⁶⁵ by weak electrolyte and interstitial pair mechanisms. LaCourse ¹⁶⁶ claimed a structural origin of the MAE in that ion motion is ¹⁶⁷ site-specific, rather than path-specific, arguing that alkali ions ¹⁶⁸ form their own environments and find it highly difficult to hop ¹⁶⁹ to other alkali sites ("defect formation"). ⁴³

Bunde⁴⁴ and Ingram^{3,45} both build on a theory similar to 171 that of LaCourse. The dynamic structure model considers that 172 alkalies have individualized sites which relax to suit their 173 inhabitants. When the alkali leaves the site, the site retains 174 "memory" of that ion, making it difficult for ions of the other 175 type to hop into it. This means pathways for ion diffusion are 176 limited to sites of that ion type, and are dependent on 177 relaxation of those sites in order to form new diffusion 178 pathways.^{3,44,45} So-called "mixed defects", an alkali sitting in an 179 unlike site, are increasingly less likely to form with increasing 180 size ratio, consistent with experiment.³

For further information on the subject beyond the largely 182 modern scope of the preceding discussion, the reader is urged 183 to consult one of many other works which have also conducted 184 thorough review of the subject. 2,3,10,11,35,43-47

Stress and strain in the network forms a common thread 186 through much of the modern experimental and computational 187 literature and many recent theoretical models either rest upon 188 or predict such phenomena. This has been shown to have 189 significant effects on macroscopic glass properties in recent 190 work. Herein a theoretical model is proposed based on the 191 strained topological constraint model of Potter et al. and 192 quantitative results discussed. 48

Background. *Topological Constraint Theory.* Topological 194 constraint theory 49-51 has been employed to solve many 195 problems in the field of theoretical glass design. 51-55 It has 196 successfully predicted the compositional dependence of 197

198 Vickers hardness, $^{21,56-58}$ fragility, changes in heat capacity at 199 the glass transition, and glass transition temperature 200 $(T_{\rm g})$. Using the energy landscape approach of Naumis 201 and the Adam–Gibbs model, 60 Mauro et al. showed that the 202 ratio of two glasses' configurational entropies $S_{\rm c}$ is equal to the 203 ratio of their topological degrees of freedom f per atom as 204 follows: 53,54

$$\frac{S_{c}[T_{g}(x_{r}), x_{r}]}{S_{c}[T_{g}(x), x]} = \frac{f[T_{g}(x_{r}), x_{r}]}{f[T_{g}(x), x]}$$
(1)

206 where x is some glass composition and the subscript r denotes 207 a reference value. f is given by

$$f = d - n \tag{2}$$

209 where d is the dimensionality of the network and n is the 210 number of constraints per atom. Since the systems in question 211 are macro-scale oxide glasses, d is simply 3. As shown by 212 Mauro and Gupta: 53,54

$$\frac{S_{c}[T_{g}(x_{r}), x_{r}]}{S_{c}[T_{g}(x), x]} = \frac{T_{g}(x)}{T_{g}(x_{r})}$$
(3)

214 and hence, given the average number of constraints per atom 215 (n), T_g may be expressed as

$$T_{g}(x) = \frac{(d - n[T_{g}(x_{r}), x_{r}])T_{g}(x_{r})}{d - n[T_{g}(x), x]}$$
(4)

217 There are three types of constraints considered in this work.

216

2.18

219

220

- a: linear bond stretching constraints associated with N—
 O bonds in oxide glasses, where N is some network
 former
- β : angular bond bending constraints associated with the O-N-O bond angle
- γ : the angular bond bending constraint associated with the N-O-N bond angle

225 α and β constraints govern the shape of the rigid glass former 226 polyhedra (e.g., SiO₂ tetrahedra), leaving the γ constraints to 227 govern the coupling of those polyhedra. The onset temperature 228 of a constraint is the characteristic temperature describing the 229 floppy-to-rigid transition of that constraint. The γ constraint in 230 silicate systems is of particular interest at low temperatures (up 231 to and including the glass transition) due to its relatively low 232 onset temperature, and is the primary focus of this 233 study 48,51,53,54,61,62

When the topologically predicted $T_{\rm g}$ would dip below the 235 onset temperature, of the γ constraint (T_{γ}) , as in high alkali-236 content silicate glasses, or rise above the formation temper-237 ature of the β constraint (T_{β}) , as in lithium borates, the actual 238 $T_{\rm g}$ becomes fixed at the onset temperature of the 239 constraint. Potter et al. described the origin of the 240 effect of water on $T_{\rm g}$ in silicate glasses using an extension of 241 this model, 8 suggesting that the energy of a given constraint 242 may be described by the following:

$$U_{\rm c} = \frac{3}{2} k_{\rm B} T_{\rm c} \tag{5}$$

244 where U_c is the constraint potential energy of an associated 245 constraint type c, T_c is the onset temperature for that 246 constraint, and $k_{\rm B}$ is Boltzmann's constant. This constraint 247 energy may be weakened or strengthened by interaction with

the local environment (e.g., by strain due to interstitial 248 species). 48 249

MODEL 250

Under the Gupta-Cooper theory, alkali ions are usually 251 considered to simply fill interstitial space between rigid 252 polyhedra and convert bridging oxygens to nonbridging 253 oxygens; this is assumed to be the case throughout this 254 work. S2,63 Any stress on the network from alkali must therefore 255 act on the γ constraint, since α and β constraints only affect the 256 geometry of individual polyhedra and not the interpolyhedra 257 couplings. To analyze the change in the γ constraint, a silicate 258 glass composition is utilized which has a predicted $T_{\rm g}$ below $T_{\gamma\gamma}$ 259 thus ensuring $T_{\rm g} = T_{\gamma}$ as per ref 48.

 T_{γ} lies between 450 and 500 °C in binary silicate glasses, 261 depending on which alkali modifier is present. 48 If internal 262 stresses act on the γ constraint, a corresponding change in the 263 $T_{\rm g}$ is expected in these alkali silicates, whereas if no internal 264 stresses arise from the mixing of alkali (or for compositions not 265 dominated by T_{γ}), $T_{\rm g}$ will not drop below T_{γ} 48 This explains 266 the minimal $T_{\rm g}$ MAE for low alkali-content silicate glasses 267 found by Shelby. 7 Equation 5 is used with both T_{γ} and eq 6 to 268 express the strain energy per atom required for a depression in 269 T_{γ} :

$$U_{\epsilon} = U_{\gamma 0} - U_{\gamma} = \frac{3}{2} k_{\rm B} [T_{\gamma 0} - T_{\gamma}] \tag{6}$$

where $U_{\gamma 0}$ and $T_{\gamma 0}$ are the energy and onset temperature, 272 respectively, of the unstrained γ constraint in the pure glass 273 former and U_{γ} and T_{γ} are the energy and onset temperature, 274 respectively, of the strained γ constraint in the modified glass. 275 From above, since the predicted $T_{\rm g}$ for all glasses examined 276 herein would be below T_{γ} , $T_{\gamma}=T_{\rm g}$, and therefore

$$U_{\epsilon} = \frac{3}{2} k_{\rm B} [T_{\gamma 0} - T_{\rm g}] \tag{7}$$

A number of previous models have suggested that glass 279 networks conform to the alkali species con-280 tained. $^{3,30,42,43,46,47,64-67}$ It is suggested here that each alkali 281 prefers some preferential distribution of angles between 282 tetrahedron on the network and different species introduce 283 strain due to the competing distributions. Considering that 284 alkalies are located predominantly interstitially, it becomes 285 clear that any strain from alkalies must occur in the γ 286 constraint; that is, only the angle distribution between 287 connected silica polyhedra should change. When this addi-288 tional strain energy is modeled simplistically as spring-like, the 289 onset temperature of the γ constraint is lowered according to 290 the following relationship:

$$U_{\gamma 0} = U_{\gamma} + U_{\epsilon} = \frac{3}{2} k_{\rm B} T_{\gamma} + \frac{1}{2} k (\Delta \theta)^2$$
(8) ₂₉₂

where k is the spring constant and $\Delta \theta$ is the change in the γ 293 constraint angle.

METHODS

Experimental Section. Binary and ternary sodium— 296 potassium silicate glasses were synthesized with nominal 297 compositions $0.30(y\text{Na}_2\text{O} + [1-y]\text{K}_2\text{O}) \cdot 0.70\text{SiO}_2$. Reagent- 298 grade powders of sodium carbonate, potassium carbonate, and 299 silica were thoroughly mixed in platinum crucibles in 300 stoichiometric amounts. Samples were then melted in a 301 preheated electric muffle furnace for 15 min at 1500 °C. 302

303 Postmelt weight loss was measured on an analytical balance 304 after cooling. The melt was reheated at the original melt 305 temperature for 5 min and then rapidly quenched via a twin-306 roller quench method to ensure homogeneity. The weight 307 losses of all glasses were found to be in good agreement with 308 prediction.

Quenched samples were then immediately powdered and analyzed in a PerkinElmer Diamond differential scanning calorimeter (DSC) using the following procedure:

- 1. Hold at 350 °C for 1 min.
 - 2. Heat at 10 °C per minute to 590 °C.
- 3. Hold at 590 °C for 1 min.

313

318

- 4. Cool at 10 °C per minute to 350 °C.
- 316 5. Hold at 350 °C for 1 min.
- 6. Heat at 10 °C per minute to 590 °C.
 - 7. Hold at 590 °C for 1 min.
- 8. Cool at 10 $^{\circ}$ C per minute to 350 $^{\circ}$ C.

320 This procedure was used to guarantee identical thermal 321 treatments among samples and remove any internal stress 322 remaining after the quench. Reported values were obtained 323 from the second heating curve. Glass transition temperatures 324 were determined using the onset method and are precise to 3 325 °C.

Computational. Molecular dynamics simulations were 326 327 carried out using potentials from Wang et al.⁶⁸ using canonical 328 ensembles of 3000 atoms with the composition $0.3[yNa_2O +$ $(1 - y)K_2O$]·0.7SiO₂. Compositions with y = 1, y = 0.75, y = 0.75330 0.5, y = 0.25, and y = 0 were tested. Atoms were randomly 331 distributed in a box, the volume of which was fixed to 332 correspond to the room-temperature density of the glass being 333 tested. 69-71 For intermediate compositions an additive density 334 relation was used, as density has been shown to be relatively 335 insensitive to mixed-alkali effects. Timesteps of 1 were 336 used and long-range Coulombic interactions were computed 337 using the Ewald method. Glass melts were initially held at a 338 temperature of 3000 °C for 1000 ps, then quenched from 3000 339 to 2000 °C instantaneously in the NVT ensemble and allowed 340 to equilibrate for a further 1000 ps as an NPT ensemble. Melts 341 were then quenched to form glasses at a fixed rate of 1 K/ps to 342 300 K in the NPT ensemble. The final result is shown in Figure 343 1.

The strain in the Si–O–Si bond angle was calculated by subtracting the expected additive distribution from the real distributions found in simulation. The resulting distributions were smoothed using high-order polynomial fits, and the minimum and maximum were determined. The difference between the two was taken to be the angular strain. Angle distributions are shown in Figures 2 and 3.

351 RESULTS

f2.f3

352 Results from the experimental work are in good agreement 353 with those from the literature and are shown in Table 1. Small 354 deviations from the literature of less than 5 °C are reasonable, 355 since different measurement apparatus (for example, Shelby 356 used dilatometry and Poole used fiber-elongation viscometry) 357 or thermal scan rates (Moynihan used a DSC scan rate of 20 358 °C per minute) are known to affect $T_{\rm g}$. In accordance with 359 literature results, the maximum deviation from additivity 360 occurs when alkali are present in nearly equal amounts. $^{5-8}$

Atomic positions and molecular structures from molecular 362 dynamics were recorded for a 10 ps increment at room 363 temperature for each glass studied. Using atomic positions, Si—

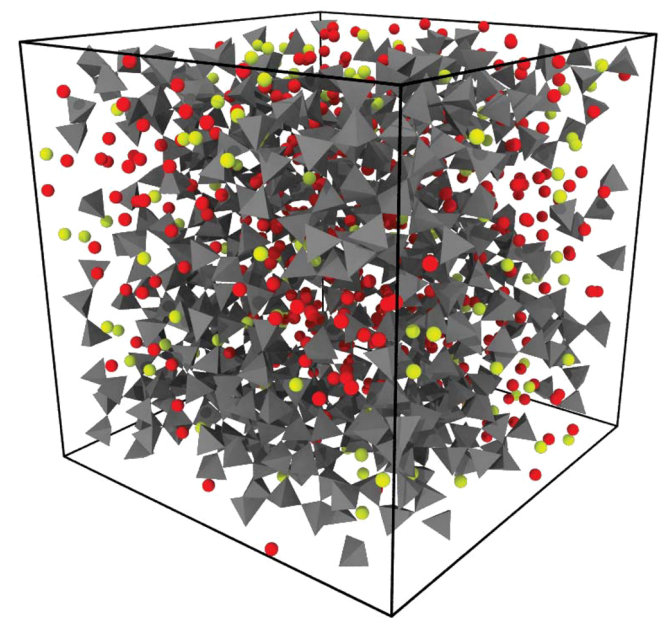


Figure 1. A simulated sodium—potassium silicate glass shown after quench (y = 0.5). Yellow and red atoms are sodium and potassium, respectively; silica tetrahedra are shown in gray.

O bond lengths (α constraint) and O–Si–O bonding angles 364 (β constraint) were calculated. The respective distributions of 365 the α and β constraints were observed to be identical across 366 compositions, as shown in Figure 2. Si–O–Si bond angles (γ 367 constraints) were also calculated, and display significant 368 bimodality when compared with the additive distribution, as 369 shown in Figure 3. These results are in excellent agreement 370 with similar simulations performed by Huang et al., who 371 reported an even greater degree of bimodality using a slower 372 quench rate. $^{37-39}$ This may also suggest that glasses with lower 373 fictive temperatures may show the MAE to a greater extent, a 374 conclusion also supported by the work of Soules and Busbey. 375

DISCUSSION

It is proposed that strain in the γ constraint is the major cause 377 for deviations from additivity observed in macroscopic 378 properties of mixed-alkali glasses. This strain has previously 379 been shown to manifest itself experimentally as a drop in T_g in 380 the T_{γ} -dominated region.⁴⁸ The presence of network strain has 381 been inferred experimentally from present DSC results and 382 literature $T_{\rm g}$ values, and computationally from molecular 383 dynamics simulations showing γ constraint angle distributions 384 that are quite bimodal compared to the additive distribution, in $_{385}$ agreement with Huang and Cormack. $_{37-39}$ Constant α and β $_{386}$ constraint values found in these simulations suggest that the 387 altered γ constraint angle distributions must be due to strain in 388 that constraint; this seems reasonable, as the γ constraint forms 389 below T_g and is less able to relax due to the high viscosity in its 390 formation range. The extent of bimodality has also been found 391 to be roughly proportional to the degree of mixing in the 392 samples.

Simulations indicate that alkali are distributed identically 394 throughout the network regardless of the degree of mixing, as 395 shown in Figure 4. However, considering the angular strain 396 f4 present in the network, it appears that each alkali species is 397 able to "customize" its local environment to its particular size 398 and shape. This suggests that the preferred site of one alkali 399

The Journal of Physical Chemistry B

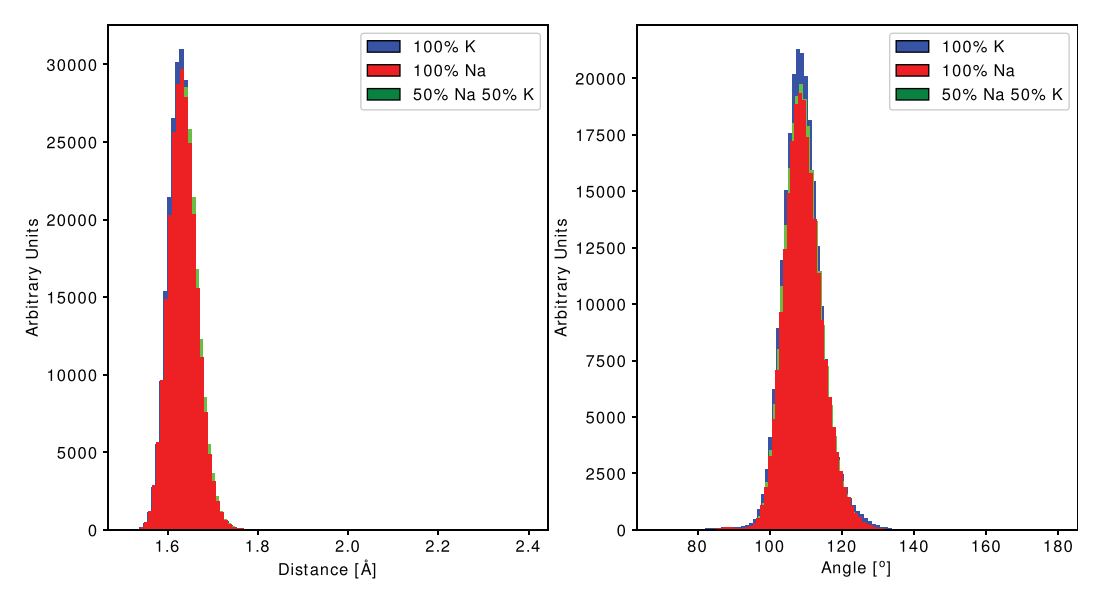


Figure 2. Left: Distribution of Si–O bond lengths (α constraint). Right: Distribution of O–Si–O bonding angles (β constraint).

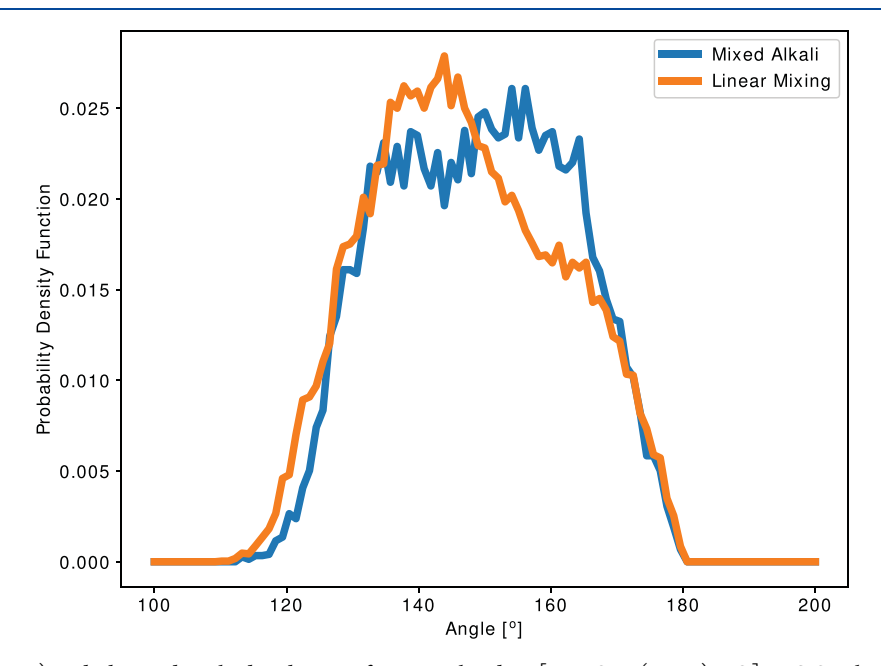


Figure 3. Expected (additive) and observed angle distributions for a simulated $0.3[yNa_2O + (1 - y)K_2O] \cdot 0.7SiO_2$ glass with y = 0.5. This same angle distribution disparity is also seen in simulations of other mixed alkali glasses.

Table 1. Experimental $T_{\rm g}$ for Synthesized Compositions Given in ${}^{\circ}{\rm C}^a$

y	$T_{\rm g}$ (°C)	Δ (°C)
0	521	0
0.17	472	-40
0.33	442	-60
0.5	430	-63
0.67	433	-50
0.83	436	-38
1	465	0

 $[^]a\Delta$ refers to the difference between the $T_{\rm g}$ which would be expected from additive mixing and that observed experimentally.

400 species puts the neighboring sites containing other alkali 401 species under stress, and vice versa. This is in agreement with 402 the experimental results of Greaves and Ngai.³⁰ Here, it is considered that the reduced potential energy of 403 the γ constraint is largely retained in the system as spring 404 potential energy. Using this approximation, topological 405 constraint theory and MD simulation data have been used to 406 calculate an effective spring constant for the γ constraint. Using 407 the average shift of bond angles from MD and the deviation of 408 experimentally measured depressed glass transition temper- 409 atures from theoretical additive values at y=0.09, a spring 410 constant of $\frac{k}{k_{\rm B}} \approx 0.52$ was obtained using an empirical fit. This empirical spring constant allows for the calculation of the 412 predicted $T_{\rm g}$ of the tested systems, which shows excellent 413 agreement with experimental data as seen in Figure 5.

Yu et al.^{40,41} found that alkali in simulated mixed-alkali 415 silicate glasses experience significant stress from the surround- 416 ing network. The network therefore must experience a 417 corresponding stress and resulting strain, distorting the 418

The Journal of Physical Chemistry B

436

463

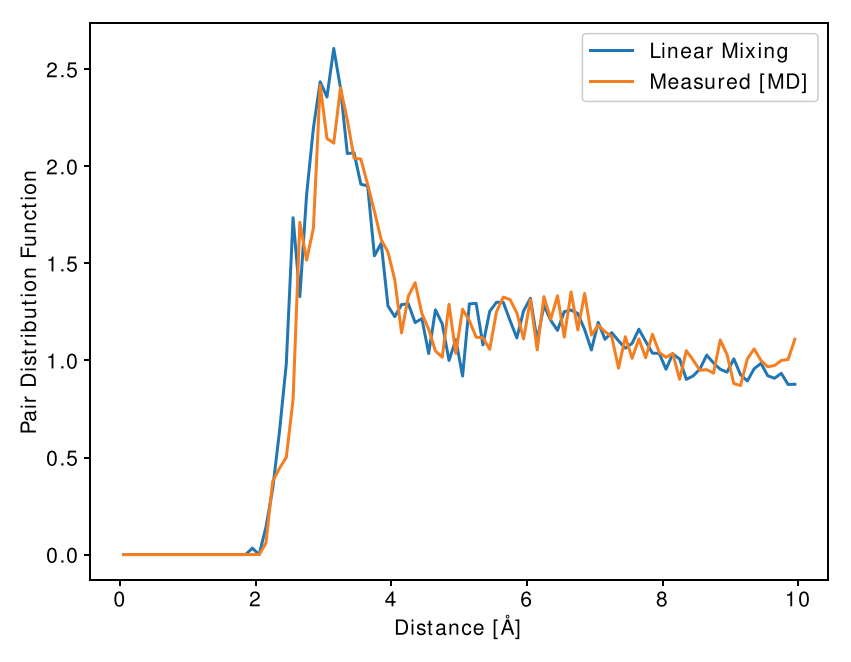


Figure 4. Alkali-alkali partial radial distribution functions (RDF) of a theoretical additive potassium-sodium silicate glass (the average RDF of two simulated binary glasses) and that of a simulated mixed-alkali glass.

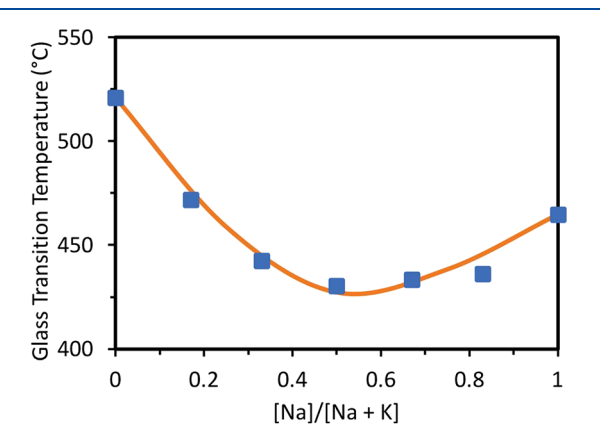


Figure 5. $T_{\rm g}$ versus sodium ion fraction for sodium—potassium silicates containing 30 mol % alkali. The orange line is the prediction from the shift in the angles calculated from simulations using $\frac{k}{k_{\rm B}}=0.09$ K and the points are present data from DSC measurements (error bars for experimental data are smaller than the points).

419 network, as observed in the presently reported bimodal 420 (strained) γ constraint distribution. During quench, alkali-421 containing interstices relax to the minimal energy state for that 422 alkali, but since the alkali distribution in mixed-alkali glasses is 423 uniform (as shown by ref 30 and in Figure 4), nearby 424 interstices containing alkali of different species relax in competition, resulting in strain on the network as inferred 426 from 40,41 above. This strain lowers the energy of the 427 corresponding γ constraint and is analogous to that from 428 molecular H 2O in hydrated glass as per ref 48 which showed 429 that constraint energies are not constant throughout the entire 430 composition range, resulting in the alteration of T_{ν} and therefore $T_{\rm g}$. The negative enthalpies of mixing observed by Lezzi and Tomozawa are well-explained by the competitive 433 relaxation and opposing stresses described above, which results 434 in an indirect attractive interaction and increased relaxation 435 driving force for $T_f - T > 0$, as found by Yu et al. ^{40,41}

CONCLUSION

During quench, mixed-alkali glass interstices relax to better 437 conform to the residing alkali. Interstices containing 438 mismatched alkali species relax toward different ultimate 439 structures, however, and the competition between these 440 interstices results in stress on the network as observed in 441 simulations by Yu et al. 40,41 and predicted by ionic motion- 442 based theoretical models. 3,43,45 The network strain model 443 described herein has been shown to have excellent quantitative 444 agreement with experimental $T_{\rm g}$ and good qualitative agree- 445 ment with a number of observations and models for the mixed- 446 alkali effect

The compositional dependence of constraint energies as a 448 result of network strain as introduced by Potter et al. 48 is 449 proposed as the mechanism responsible for the mixed alkali 450 effect. New results for mixed-alkali silicate glass transition 451 temperatures have been presented, as well as molecular 452 dynamics simulations showing uniform alkali distributions, 453 unmodified α and β constraints, and bimodal γ constraint 454 distributions for mixed-alkali silicates as compared with binary 455 alkali silicate glasses, all in good agreement with liter- 456 ature. 30,37-39 Finally, experimental observations of the mixed 457 alkali effect in the glass transition temperature have been 458 explicated quantitatively in terms of a topological model with 459 strained Si-O-Si bond angles.

The implications of this model on ionic conductivity are 461 currently under investigation.

AUTHOR INFORMATION

Corresponding Author 464 *E-mail: jcm426@psu.edu. 465 ORCID □ 466 Qiuju Zheng: 0000-0003-3785-1709 467 Mathieu Bauchy: 0000-0003-4600-0631 468 John C. Mauro: 0000-0002-4319-3530 469 Notes 470 The authors declare no competing financial interest. 471

544

561

563

580

472 **ACKNOWLEDGMENTS**

473 The authors wish to acknowledge Ozgur Gulbiten for his 474 insightful comments. Funding for experimental work was 475 provided to Coe College by the NSF through Division of 476 Materials Research Grant 1746230.

REFERENCES

- (1) Weber, R. Uber Den Einfluß Der Zusammensetzung Des Glases 479 Auf Die Depressions- Erscheinungen Der Thermometer. Berliner 480 Akad. Wiss. 1883, 2, 1233-1238.
- (2) Dietzel, A. H. On the So-Called Mixed Alkali Effect. Physics and 481 482 chemistry of glasses 1983, 24, 172-180.
- (3) Ingram, M. D. The Mixed Alkali Effect Revisited-a New Look at 483 484 an Old Problem. Glastechnische Berichte 1994, 67, 151-155.
- (4) Sheybany, H. A. De La Structure Des Verres Alkalinosilicates 486 Mixtes. Verres et Refractaires 1948, 2, 127-145.
- (5) Poole, J. P. Low-Temperature Viscosity of Alkali Silicate Glasses. 487 488 J. Am. Ceram. Soc. 1949, 32, 230-233.
- (6) Moynihan, C. T.; Easteal, A. J.; Tran, D. C.; Wilder, J. A.; 490 Donovan, E. P. Heat Capacity and Structural Relaxation of Mixed-491 Alkali Glasses. J. Am. Ceram. Soc. 1976, 59, 137-140.
- (7) Shelby, J. E. Thermal Expansion of Mixed-Alkali Silicate Glasses. 493 J. Appl. Phys. 1976, 47, 4489-4496.
- (8) Bershtein, V. A.; Gorbachev, V. V.; Egorov, V. M. Structure 494 495 Peculiarities of Mixed Alkali Silicate Glasses. J. Non-Cryst. Solids 1980, 496 38-39, 141-146,
- (9) Berkemeier, F.; Voss, S.; Imre, A. W.; Mehrer, H. Molar Volume, 498 Glass-Transition Temperature, and Ionic Conductivity of Na- and Rb-499 Borate Glasses in Comparison with Mixed Na-Rb Borate Glasses. J. 500 Non-Cryst. Solids 2005, 351, 3816-3825.
- (10) Isard, J. The Mixed Alkali Effect in Glass. J. Non-Cryst. Solids 501 502 1969, 1, 235-261.
- (11) Day, D. E. Mixed Alkali Glasses Their Properties and Uses. J. 503 504 Non-Cryst. Solids 1976, 21, 343-372.
- (12) Welch, R. C.; Smith, J. R.; Potuzak, M.; Guo, X.; Bowden, B. F.; 506 Kiczenski, T. J.; Allan, D. C.; King, E. A.; Ellison, A. J.; Mauro, J. C.
- 507 Dynamics of Glass Relaxation at Room Temperature. Phys. Rev. Lett. 508 2013, 110, 265901.
- (13) Balaya, P.; Sunandana, C. S. Mixed Alkali Effect in the 30[(1 -510 x)Li2O · xNa2O]: 70TeO2glass System. J. Non-Cryst. Solids 1994, 511 175, 51-58.
- 512 (14) Komatsu, T.; Noguchi, T.; Benino, Y. Heat Capacity Changes 513 and Structural Relaxation at Glass Transition in Mixed-Alkali Tellurite 514 Glasses. J. Non-Cryst. Solids 1997, 222, 206-211.
- (15) Komatsu, T.; Noguchi, T.; Sato, R. Heat Capacity Changes at 516 the Glass Transition in Mixed-Alkali Telluite Glasses. J. Am. Ceram. 517 Soc. 1997, 80, 1327-1332.
- (16) Kuppinger, C. M.; Shelby, J. E. Viscosity and Thermal 519 Expansion of Mixed-Alkali Sodium-Potassium Borate Glasses. J. Am. 520 Ceram. Soc. 1985, 68, 463-467.
- (17) McVay, G. L.; Day, D. E. Diffusion and Internal Friction in 521 Single-Alkali Glasses. J. Am. Ceram. Soc. 1970, 53, 284-285. 522
- (18) Fleming, J. W.; Day, D. E. Relation of Alkali Mobility and 524 Mechanical Relaxation in Mixed-Alkali Silicate Glasses. J. Am. Ceram. 525 Soc. 1972, 55, 186-192.
- (19) Lezzi, P. J.; Tomozawa, M. Enthalpy of Mixing of Mixed Alkali 526 527 Glasses. J. Non-Cryst. Solids 2010, 356, 1439-1446.
- (20) Lezzi, P. J.; Tomozawa, M. Effect of Alumina on Enthalpy of 528 529 Mixing of Mixed Alkali Silicate Glasses. J. Non-Cryst. Solids 2011, 357, 530 2086-2092.
- (21) Yu, Y.; Wang, M.; Anoop Krishnan, N.; Smedskjaer, M. M.; 532 Deenamma Vargheese, K.; Mauro, J. C.; Balonis, M.; Bauchy, M.
- 533 Hardness of Silicate Glasses: Atomic-Scale Origin of the Mixed 534 Modifier Effect. J. Non-Cryst. Solids 2018, 489, 16-21.
- (22) Mohajerani, A.; Zwanziger, J. Mixed Alkali Effect on Vickers
- 536 Hardness and Cracking. J. Non-Cryst. Solids 2012, 358, 1474-1479.

- (23) Jain, H.; Peterson, N.; Downing, H. Tracer Diffusion and 537 Electrical Conductivity in Sodium-Cesium Silicate Glasses. J. Non- 538 Cryst. Solids 1983, 55, 283-300.
- (24) Jain, H.; Downing, H. L.; Peterson, N. L. The Mixed Alkali 540 Effect in Lithium-Sodium Borate Glasses. J. Non-Cryst. Solids 1984, 541 64. 335-349. 542
- (25) Terai, R. The Mixed Alkali Effect in the Na2OCs2OSiO2 543 Glasses. I. Non-Cryst. Solids 1971, 6, 121-135.
- (26) Tomozawa, M.; Yoshiyagawa, M. Ac Electric Characteristic of 545 Mixed Alkali Glasses. Glastech. Ber. 1983, 56, 939-44.
- (27) Schoo, U.; Cramer, C.; Mehrer, H. Tracer Diffusion in Sodium 547 - Rubidium Borate Glasses. Solid State Ionics 2000, 138, 105-114. 548
- (28) Schoo, U.; Cramer, C.; Ratai, E.; Mehrer, H. Diffusion in Single 549 and Mixed-Alkali Borate Glasses. Defect Diffus. Forum 2001, 194-199, 550
- (29) Tomozawa, M.; McGahay, V. Mechanism of the Mixed Alkali 552 Effect Based upon the Thermodynamic State of Glass. J. Non-Cryst. 553 Solids 1991, 128, 48-56. 554
- (30) Greaves, G.; Ngai, K. Ionic Transport Properties in Oxide 555 Glasses Derived from Atomic Structure. J. Non-Cryst. Solids 1994, 556 172-174, 1378-1388,
- (31) Swenson, J.; Matic, A.; Karlsson, C.; Borjesson, L.; Meneghini, 558 C.; Howells, W. S. Random Ion Distribution Model: A Structural 559 Approach to the Mixed-Alkali Effect in Glasses. Phys. Rev. B: Condens. 560 Matter Mater. Phys. 2001, 63, 132202.
- (32) Swenson, J.; Adams, S. Mixed Alkali Effect in Glasses. Phys. Rev. 562 Lett. 2003, 90, 155507.
- (33) Kamitsos, E. I.; Patsis, A. P.; Chryssikos, G. D. Interactions 564 between Cations and the Network in Mixed Alkali Borate Glasses. 565 Phys. Chem. Glasses 1991, 32, 219.
- (34) Sen, S.; George, A. M.; Stebbins, J. F. Ionic Conduction and 567 Mixed Cation Effect in Silicate Glasses and Liquids:23Na and7Li 568 NMR Spin-Lattice Relaxation and a Multiple- Barrier Model of 569 Percolation. J. Non-Cryst. Solids 1996, 197, 53-64.
- (35) Tomozawa, M. Structure of Mixed Alkali Glasses. J. Non-Cryst. 571 Solids 1996, 196, 280-284.
- (36) Habasaki, J.; Ngai, K. L. The Mixed Alkali Effect in Ionically 573 Conducting Glasses Revisited: A Study by Molecular Dynamics 574 Simulation. Phys. Chem. Chem. Phys. 2007, 9, 4673-4689.
- (37) Huang, C.; Cormack, A. N. The Structure of Sodium Silicate 576 Glass. J. Chem. Phys. 1990, 93, 8180-8186.
- (38) Huang, C.; Cormack, A. N. Structural Differences and Phase 578 Separation in Alkali Silicate Glasses. J. Chem. Phys. 1991, 95, 3634-579 3642.
- (39) Huang, C.; Cormack, A. N. Structure and Energetics in Mixed- 581 Alkali-Metal Silicate Glasses from Molecular Dynamics. J. Mater. 582 Chem. 1992, 2, 281-287. 583
- (40) Yu, Y.; Wang, M.; Zhang, D.; Wang, B.; Sant, G.; Bauchy, M. 584 Stretched Exponential Relaxation of Glasses at Low Temperature. 585 Phys. Rev. Lett. 2015, 115, 165901.
- (41) Yu, Y.; Wang, M.; Smedskjaer, M. M.; Mauro, J. C.; Sant, G.; 587 Bauchy, M. Thermometer Effect: Origin of the Mixed Alkali Effect in 588 Glass Relaxation. Phys. Rev. Lett. 2017, 119, 095501. 589
- (42) Anderson, O. L.; Stuart, D. A. Calculation of Activation Energy 590 of Ionic Conductivity in Silica Glasses by Classical Methods. J. Am. 591 Ceram. Soc. 1954, 37, 573-580. 592
- (43) LaCourse, W. C. A Defect Model for the Mixed Alkali Effect. J. 593 Non-Cryst. Solids 1987, 95-96, 905-912. 594
- (44) Bunde, A.; Ingram, M.; Maass, P.; Ngai, K. Mixed Alkali Effects 595 in Ionic Conductors: A New Model and Computer Simulations. J. 596 Non-Cryst. Solids 1991, 131, 1109-1112.
- (45) Ingram, M. D. Ionic Conductivity in Glass. Phys. Chem. Glasses 598 1987, 28, 215-234. 599
- (46) Hunt, A. The Mixed-Alkali Effect Discussed within the Context 600 of Percolative Transport. J. Non-Cryst. Solids 1997, 220, 1-16. 601
- (47) Hunt, A. Mixed-Alkali Effect: Some New Results. J. Non-Cryst. 602 Solids 1999, 255, 47-55.

The Journal of Physical Chemistry B

- 604 (48) Potter, A. R.; Wilkinson, C. J.; Kim, S. H.; Mauro, J. C. Effect of 605 Water on Topological Constraints in Silica Glass. *Scr. Mater.* **2019**, 606 *160*, 48–52.
- 607 (49) Phillips, J. C. Topology of Covalent Non-Crystalline Solids: 608 Short-Range Order in SeyGexSb1-x-Yalloys. *J. Non-Cryst. Solids* 1979, 609 34, 153–181.
- 610 (50) Phillips, J. C.; Thorpe, M. F. Constraint Theory, Vector 611 Percolation and Glass Formation. *Solid State Commun.* **1985**, 53, 612 699–702.
- 613 (51) Mauro, J. C. Topological Constraint Theory of Glass. Am. 614 Ceram. Soc. Bull. 2011, 90, 31–37.
- 615 (52) Gupta, P. K.; Cooper, A. R. Topologically Disordered 616 Networks of Rigid Polytopes. *J. Non-Cryst. Solids* **1990**, *123*, 14–21.
- 617 (53) Gupta, P. K.; Mauro, J. C. Composition Dependence of Glass
- 618 Transition Temperature and Fragility. I. A Topological Model 619 Incorporating Temperature-Dependent Constraints. *J. Chem. Phys.* 620 **2009**, *130*, No. 094503.
- 621 (54) Mauro, J. C.; Gupta, P. K.; Loucks, R. J. Composition 622 Dependence of Glass Transition Temperature and Fragility. II. A 623 Topological Model of Alkali Borate Liquids. *J. Chem. Phys.* **2009**, *130*, 624 234503.
- 625 (55) Mauro, J. C.; Tandia, A.; Vargheese, K. D.; Mauro, Y. Z.; 626 Smedskjaer, M. M. Accelerating the Design of Functional Glasses 627 through Modeling. *Chem. Mater.* **2016**, 28, 4267–4277.
- 628 (56) Bauchy, M.; Javad Abdolhosseini Qomi, M.; Bichara, C.; Ulm, 629 F.-J.; J-M Pellenq, R. Rigidity Transition in Materials: Hardness is 630 Driven by Weak Atomic Constraints. *Phys. Rev. Let.* **2015**, *114*, 631 125502.
- 632 (57) Smedskjaer, M. M.; Mauro, J. C.; Youngman, R. E.; Hogue, C. 633 L.; Potuzak, M.; Yue, Y. Topological Principles of Borosilicate Glass 634 Chemistry. *J. Phys. Chem. B* **2011**, *115*, 12930–12946.
- 635 (58) Zheng, Q.; Yue, Y.; Mauro, J. C. Density of Topological 636 Constraints as a Metric for Predicting Glass Hardness. *Appl. Phys.* 637 Lett. 2017, 111, No. 011907.
- 638 (59) Bauchy, M.; Micoulaut, M. Atomic Scale Foundation of 639 Temperature-Dependent Bonding Constraints in Network Glasses 640 and Liquids. *J. Non-Cryst. Solids* **2011**, 357, 2530–2537.
- 641 (60) Naumis, G. G. Glass Transition Phenomenology and 642 Flexibility: An Approach Using the Energy Landscape Formalism. *J.* 643 *Non-Cryst. Solids* **2006**, 352, 4865–4870.
- 644 (61) Mauro, J. C. Decoding the Glass Genome. *Curr. Opin. Solid* 645 *State Mater. Sci.* **2018**, 22, 58–64.
- 646 (62) Zheng, Q.; Mauro, J. C.; Yue, Y. Reconciling Calorimetric and 647 Kinetic Fragilities of Glass-Forming Liquids. *J. Non-Cryst. Solids* **2017**, 648 456, 95–100.
- 649 (63) Zachariasen, W. H. The Atomic Arrangement in Glass. *J. Am.* 650 *Chem. Soc.* **1932**, *54*, 3841–3851.
- 651 (64) Lengyel, B.; Boksay, Z. Uber Die Elektrische Leitfahigkeit Des 652 Glases I. Z. Phys. Chem. **1953**, 93.
- 653 (65) Stevels, J. Experiments and Theories on the Power Factor of 654 Glasses as a Function of Composition: II. *Verres et Refractaires* **1951**, 655 5, 4–14.
- 656 (66) Maass, P.; Bunde, A.; Ingram, M. D. Ion Transport Anomalies 657 in Glasses. *Phys. Rev. Lett.* **1992**, *68*, 3064–3068.
- 658 (67) Kirchheim, R. The Mixed Alkali Effect as a Consequence of 659 Network Density and Site Energy Distribution. *J. Non-Cryst. Solids* 660 **2000**, 272, 85–102.
- 661 (68) Wang, M.; Anoop Krishnan, N. M.; Wang, B.; Smedskjaer, M.
- 662 M.; Mauro, J. C.; Bauchy, M. A New Transferable Interatomic 663 Potential for Molecular Dynamics Simulations of Borosilicate Glasses.
- 664 J. Non-Cryst. Solids 2018, 498, 294-304.
- 665 (69) Doweidar, H. Mixed Modifier Glasses: A New View as Mixed 666 Matrices. *J. Mater. Sci.* **2013**, *48*, 7736–7742.
- 667 (70) Giri, S.; Gaebler, C.; Helmus, J.; Affatigato, M.; Feller, S.; 668 Kodama, M. A General Study of Packing in Oxide Glass Systems
- 669 Containing Alkali. J. Non-Cryst. Solids 2004, 347, 87–92.
- 670 (71) Tischendorf, B.; Ma, C.; Hammersten, E.; Venhuizen, P.; 671 Peters, M.; Affatigato, M.; Feller, S. The Density of Alkali Silicate

Glasses Over Wide Compositional Ranges. J. Non-Cryst. Solids 1998, 672 239, 197–202.